Song Cheng, Libo Zhang, Hongying Xia* and Jinhui Peng

Characterization and adsorption properties of La and Fe modified activated carbon for dye wastewater treatment

DOI 10.1515/gps-2016-0120
Received August 17, 2016; accepted October 26, 2016; previously published online March 23, 2017

Abstract: An effective adsorbent (Fe-La-AC) was synthesized by impregnating mixed solution ferric nitrate and lanthanum nitrate with activated carbon and heated by microwave to remove methylene blue (MB) from dye wastewater. The Fe-La-AC was characterized by N_2 adsorption, Fourier transform infrared spectroscopy, Raman, X-ray diffraction (XRD), X-ray photoelectron spectroscopy, and scanning electron microscopy. Moreover, the existence of Fe_3O_4 leads to Fe-La-AC having magnetic properties, which makes it easily separated and recycled from dye wastewater in an external magnetic field. After modification, the following phenomena occurred: Brunauer-Emmett-Teller surface area, average pore diameter, and total pore volume decreased; graphitization degree decreased. In addition, the equilibrium isotherms and kinetics of MB adsorption on raw activated carbon and Fe-La-AC were examined. The equilibrium adsorption data indicated that the adsorption behavior followed the Langmuir isotherm, and the pseudo-second-order model matched well the kinetic data. The maximum adsorption capacity of Fe-La-AC is 261.10 mg/g, which increases by 26.38% as compared with raw activated carbon. According to these results, Fe-La-AC is a promising adsorbent for the removal of MB from dye wastewater.

Keywords: adsorption; Fe-La-AC; synthesis; wastewater.

***Corresponding author: Hongying Xia,** State Key Laboratory of Complex Nonferrous Metal Resources Clean Utilization, Kunming University of Science and Technology, Wen Chang Road 86, Wuhau District, Yunnan 650093, China; Yunnan Provincial Key Laboratory of Intensification Metallurgy, Kunming University of Science and Technology, Kunming, Yunnan 650093, China; National Local Joint Laboratory of Engineering Application of Microwave Energy and Equipment Technology, Kunming, Yunnan 650093, China; and Faculty of Metallurgical and Energy Engineering, Kunming University of Science and Technology, Kunming 650093, China, e-mail: hyxia@kmust.edu.cn
Song Cheng, Libo Zhang and Jinhui Peng: State Key Laboratory of Complex Nonferrous Metal Resources Clean Utilization, Kunming University of Science and Technology, Kunming, Yunnan 650093, China; Yunnan Provincial Key Laboratory of Intensification Metallurgy, Kunming University of Science and Technology, Kunming, Yunnan 650093, China; National Local Joint Laboratory of Engineering Application of Microwave Energy and Equipment Technology, Kunming, Yunnan 650093, China; and Faculty of Metallurgical and Energy Engineering, Kunming University of Science and Technology, Kunming 650093, China

1 Introduction

Dyes are coloring agents used by varieties of industries, including textile, plastics, and paper and pulp, among others, to colorize their final products. A total of 30% of the world production of dyes may be lost during dyeing process, and most dyes are toxic [1]. The dye residues that were uncontrolled and released as industrial wastewater into the water streams have led to several negative effects, including a decrease in light penetration and carcinogenic and mutagenic changes to organisms [2]. The dye wastewater can also cause allergy, dermatitis, and skin irritation and can also provoke cancer and mutation in humans [3–5]. Therefore, large content of dyes in wastewater must be treated before discharge into environment, as to minimize the threat to the environmental problems and harmful hazards [4, 5]. However, the dyes are more difficult to biodegrade and remove from dye wastewater because of their high solubility in water and complex aromatic molecular structures [6, 7]. Thus, providing an effective method to control and govern dye wastewater becomes highly urgent.

Various physical and chemical treatment methods, including coagulation [8], reverse osmosis [9], photodegradation [10], chemical oxidation [11], membrane filtration method [12], ozonation [13], and biosorption [14], are used to treat dye wastewater. However, these methods are generally ineffective or have high operating costs on dye treatment. To date, adsorption treatment is considered to be green, to have high efficiency, to have low cost, and to ease the procedure for dye wastewater treatment [15]. Activated carbon, an abundant porous structure and a strong adsorption capacity material, is widely used in many different industries, including in separation, catalyst supports, and removal of dyes and pollutants from wastewater [15–17]. It is capable of adsorbing many kinds of dyes with a high

adsorption capacity, but its adsorption efficiency is low. These disadvantages restrict their extensive application.

To overcome these disadvantages, more and more attention has been paid on the modification of activated carbon and synthesis of high-performance adsorbents to treat dye wastewater. This process is an effective route to improve the removal efficiency of activated carbon for various pollutants [18]. Dong et al. [19] prepared a kind of adsorbent of ferromagnetic-ordered mesoporous carbons via chemical activation and then followed by the reduction of solution ferric nitrate under N_2 condition with high adsorption on bulky dye molecules. Goscianska et al. [20] reported a kind of mesoporous carbon materials modified with lanthanum(III) chloride having good performance in the treatment of methyl orange dye from wastewater. Shah et al. [21] also prepared FeAC material via iron-doped activated carbon. FeAC has shown up to 98% methylene blue (MB) removal from the aqueous media. According to literature reported, La has been already successfully impregnated with activated carbon or mesoporous silicate materials for wastewater treatment [22]. Wang et al. [22] have synthesized La-BC with La loaded into biochar, which achieved the high removal efficiency of phosphate from wastewater. More recently, activated carbon impregnated with lanthanum oxide was synthesized and applied for convert NO to N_2 as catalysts because of its high affinity to the functional groups into activated carbon [23]. Iron oxides are also regarded as a promising material in dye wastewater treatment. Kadirova et al. [24] have prepared Fe_2O_3-activated carbons having good performance removal of MB from wastewater. Although many studies have been devoted to preparing highly effective adsorbents, adsorbents with single metal oxide have some disadvantages. Recently, prepared composite adsorbents impregnated with two or more different metal oxides have attracted great attention. The reason is that they have the advantages of different kinds of metal oxides as compared with adsorbents prepared with single metal oxide [25]. In addition, they could have the synergistic effect that greatly increases their adsorption performance [26].

In general, there are two basic heating methods to modify activated carbon and to synthesize the composite adsorbent: conventional heating and microwave heating. Conventional heating is widely used to heating the material. However, the heat generated by conventional heating methods does not ensure a uniform temperature as it is based on heat transfer through conduction and convection [27]. Fortunately, the disadvantages of the conventional heating are overcame by a new heating method: microwave heating. Microwave heating is molecular level heating, and the heat is generated from inside the material as the materials receive energy through dipole rotations and ionic conduction [28]. Compared with conventional heating, microwave heating has been proven beyond doubt to possess qualities such as fast heating, energy efficient, easy control, small thermal inertia, and selective heating. Thus, we chose the microwave heating to synthesize Fe-La-AC.

However, to the best of our knowledge, there have been a limited number of studies regarding synthesizing Fe-La-AC composite on the surface of activated carbon for dye wastewater treatment via microwave heating based on their advantages. In this work, we put forward a technical route in which raw activated carbon was treated with ultrasound and impregnated with ferric nitrate and lanthanum nitrate, forming a kind of composite adsorbent (Fe-La-AC) by microwave heating. Cationic organic dye MB is a kind of basic dye widely used in the above-mentioned industrial application. Therefore, MB is selected as the model pollutant to test the removal performance of the Fe-La-AC. Besides, we also thoroughly studied the adsorption process of Fe-La-AC. Both raw activated carbon and Fe-La-AC were characterized by using several characterization techniques.

2 Materials and methods

Raw activated carbon was purchased by Chengdu Kelon Chemical Reagent Factory of China. Chemical reagents, including $Fe(NO_3)_3$ (Tianjin Regent Chemicals Co., Ltd., China), $La(NO_3)_3$ (Tianjin Regent Chemicals Co., Ltd.), and MB (Tianjin Standard Technology Company, China), were all analytical grade. The raw activated carbon was treated by ultrasound (Baoding city one electronic equipment co., Ltd, Heibei, China) for 30 min (ultrasound-activated carbon) to clean the impurities on the surface of carbon via ultrasonic cavitation. Then 15 g of dry ultrasound-activated carbon was placed in a 150-ml Erlenmeyer flask with $Fe(NO_3)_3/La(NO_3)$ mole ratios of 5 : 1, 4 : 2, 3 : 3, 2 : 4, and 1 : 5 (using 0.1 mol/l of $Fe(NO_3)_3$ and $La(NO_3)_3$ solution mixed) for 3 h. Then the suspensions were filtered and dried at 105°C for 24 h. Finally, the sample was heated in a microwave (National Local Joint Laboratory of Engineering Application of Microwave Energy and Equipment Technology, Kunming, Yunnan, China) furnace with a microwave power of 700 W, a temperature of 700°C, and a heating time of 25 min. A multimode continuous controllable microwave power was used in the microwave furnace for the experiments. As Figure 1 shows, the largest MB adsorption of Fe-La-AC is 265 mg/g with a $Fe(NO_3)_3/La(NO_3)_3$ ratio of 4 : 2. Thus, a $Fe(NO_3)_3/La(NO_3)$ mole ratio of 4 : 2 was chosen to do the further experiment. Table 1 lists the industry analysis on raw activated carbon and ultrasound-activated carbon. As shown in Table 1, the fixed carbon of the ultrasound-activated carbon increases and other ingredients decrease because of ultrasonic cavitation, contributing to impregnated $Fe(NO_3)_3$ and $La(NO_3)_3$.

2.1 Characterization of Fe-La-AC

The N_2 adsorption of Fe-La-AC was conducted at 77 K using an automatic adsorption apparatus (Autosorb-1-C, USA) with relative

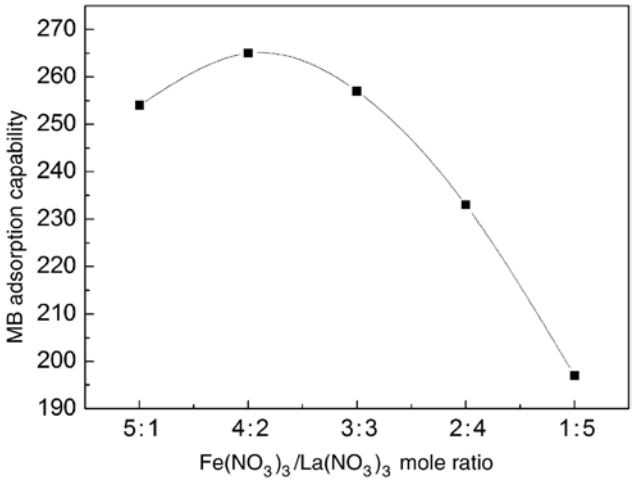

Figure 1: The effect of mole ratio on the adsorption capability of Fe-La-AC.

Table 1: Industry analysis on raw activated carbon and ultrasound-activated carbon.

	Ash (%)	Volatile (%)	Moisture (%)	Fixed carbon (%)
Raw activated carbon	3.29	3.99	1.9	92.72
Ultrasound-activated carbon	2.28	3.65	1.5	94.06

pressure (P/P_0) ranging from 10^{-7} to 1. The total pore volumes were estimated to be the equivalent liquid volume of the adsorbate (N_2) at a relative pressure of 0.99. The Brunauer-Emmett-Teller (BET) surface area of the samples was calculated by the BET equation. Pore size distribution was analyzed by using the nonlocal density functional theory. Scanning electron microscopy (SEM; Philips XL30ESEM-TMP) analysis was used to assess the surface morphology. The Fourier transform infrared (FTIR) spectroscopy (Nicolet iS10, USA) was applied to qualitatively identify the chemical function groups of samples. The Raman analysis for the samples was conducted by Ramascope System 1000 (Renishaw, UK) spectroscopy with a laser excitation wavelength of 514.5 nm. Powder X-ray diffractometer was equipped with Cu Kα X-ray source at 40 kV and 40 mA (D/max-3B, Japan). X-ray photoelectron spectroscopy (XPS) was performed on a PHI 5500 electron spectrometer (Physical Electronics, Inc., Chanhassen, MN, USA) using 200-W Mg radiations.

2.2 Adsorption experiments

The equilibrium isotherms of MB adsorption on raw activated carbon and Fe-La-AC were conducted by batch adsorption tests in 150-ml Erlenmeyer flasks. Fifty milliliters of MB solutions with different initial concentrations (200–600 mg/l) was placed in each Erlenmeyer flask. Each 0.1 g of raw activated carbon and Fe-La-AC with a particle size of 71 μm was added to each Erlenmeyer flask and kept in a thermostat oscillator with a shaking speed of 300 rpm at different temperatures (30°C and 40°C) until adsorption equilibrium was reached. After equilibrium was attained, the amount of residual MB concentration was conducted at 668 nm by a UV-vis spectrophotometer. The amount of MB in adsorbents, q_e (mg/g), was obtained under equilibrium conditions of the following equation:

$$q_e = (C_0 - C_e)V/M, \quad (1)$$

where C_0 (mg/l) is the initial concentration of MB and C_e (mg/l) is the equilibrium concentration of MB. V and M are the volume of the solution (l) and the weight of the adsorbents (g), respectively.

Three famous isotherm models, Langmuir, Freundlich, and Temkin, were applied to fit the adsorption data [27, 28]. The parameters of these models are presented in Table 2.

Kinetic studies were also conducted using 150-ml Erlenmeyer flasks; the methods are almost similar to isotherm studies. The Erlenmeyer flasks with MB and adsorbents were taken at different time intervals. The amount of MB adsorbed over time, q_t (mg/g), was obtained by using the following equation:

$$q_t = (C_0 - C_t)V/M, \quad (2)$$

where C_t (mg/l) is the liquid-phase concentration of MB solution at time t (min). In this work, three different models such as pseudo-first-order model, pseudo-second-order model, and intraparticle diffusion model were applied to interpret the kinetic data [27]. The parameters of three models are listed in Table 3.

3 Results and discussion

3.1 Characterizations of pore structure

Figure 2 shows (A) the nitrogen adsorption isotherms of ultrasound-activated carbon, raw activated carbon, and Fe-La-AC and the (B) pore size distribution of Fe-La-AC.

Table 2: Adsorption isotherm models adopted in this work and their parameters.

Isotherm	Equation	Parameters
Langmuir isotherm	$\frac{1}{q_e} = \frac{1}{K_L Q_0 C_e} + \frac{1}{Q_0}$	C_e is the equilibrium concentration (mg/l) Q_0 (mg/g) is the adsorption constant related to adsorption capacity K_L (l/g) is the adsorption constant related to energy of adsorption
Freundlich isotherm	$\ln(q_e) = \ln(K_F) + \frac{1}{n}\ln(C_e)$	K_F is the adsorption constant related to adsorption capacity (mg/g)·(l/mg)$^{1/n}$ n is the adsorption constant measuring the adsorption intensity
Temkin isotherm	$q_e = A + B\ln(C_e)$	A and B are constants

Table 3: Adsorption kinetic models adopted in this work and their parameters.

Kinetic models	Equation	Parameters
Pseudo-first order	$\ln(q_e - q_t) = \ln q_e - K_1 t$	q_e is the uptake of MB at equilibrium (mg/g) K_1 (1/min) is the adsorption rate constant
Pseudo-second order	$\frac{t}{q_e} = \frac{1}{K_2 q_e^2} + \frac{t}{q_e}$	K_2 (g/mg/min) is the rate constant of second-order equation
Intraparticle diffusion	$q_t = K_3\sqrt{t} + C$	K_3 (mg/g/min$^{1/2}$) is the intraparticle diffusion rate constant C is a constant

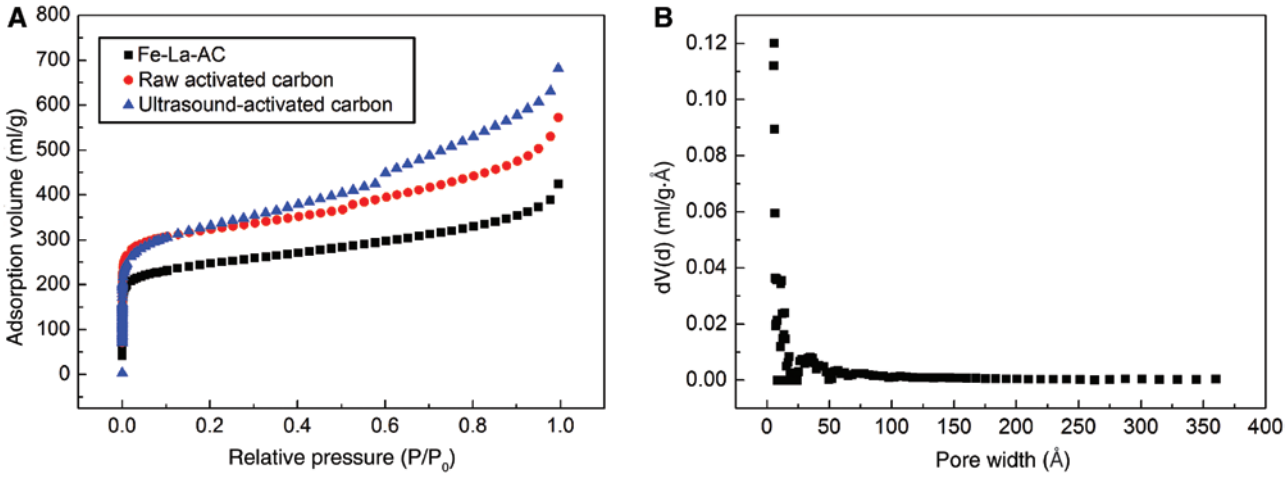

Figure 2: (A) Nitrogen adsorption isotherm of raw activated carbon, ultrasound-activated carbon, and Fe-La-AC and (B) pore distribution of Fe-La-AC.

These isotherms present between I and II according to the International Union of Pure and Applied Chemistry classification (Figure 2A). All of them exhibited a high N_2 uptake at low relative pressures ($P/P_0 < 0.1$), indicating the presence of a great deal of microporous material. As shown in Figure 2A, the BET surface area of the ultrasound-activated carbon significantly increases compared with that of raw activated carbon because of the fact that impurities in raw activated carbon are cleaned by the "cavitations" of ultrasound. Fe-La-AC is less than ultrasound-activated carbon in the BET surface area. This phenomenon is caused by pore blocking, a result of lanthanum-iron-carbon matrix interaction. Pore size distribution is also a very important property of Fe-La-AC. As shown in Figure 2B, the sharpest peak ranges from 10 to 50 Å, indicating that a majority of the pores fall into the range of mesopores. As we all know, the adsorption counts on the pore structure besides the surface chemical properties of adsorbent. Kasaoka et al. [29] reported that adsorption occurred when the pore diameter of the adsorbent is at least 1.7 times as much as that of the adsorbate. The minimum molecular size of MB is approximately 0.8 nm, whereas the average pore size of Fe-La-AC is 3.51 nm. Thus, it is accessible to adsorption MB molecule.

The pore structure and the MB removal value of activated carbons are shown in Table 4. Compared with raw activated carbon, the average pore diameter of Fe-La-AC and ultrasound-activated carbon decreases. This proves that the proportion of the microporous material of two kinds of activated carbons is higher. It is easy to find that the micropore volume of ultrasound-activated carbon is bigger than that of Fe-La-AC, based on the difference in average pore size. Although the BET, the total pore volume, and even the micropore volume of Fe-La-AC are less as compared with ultrasound-activated carbon, the MB removal value of Fe-La-AC is higher than that of ultrasound-activated carbon, proving that the iron and lanthanum compounds on the Fe-La-AC play a significance role in MB removal.

3.2 FTIR analysis

Figure 3 shows the FTIR spectra of raw activated carbon and Fe-La-AC. Some information about the chemical

Table 4: Details of pore structure and MB removal value of raw activated carbon, ultrasound-activated carbon, and Fe-La-AC.

Subject	Raw activated carbon	Ultrasound-activated carbon	Fe-La-AC
BET surface area (m^2/g)	912	1257	1013
Average pore diameter (nm)	5.51	3.07	3.51
Total pore volume (cm^3/g)	1.02	1.09	0.77
MB removal value (mg/g)	125	158	265

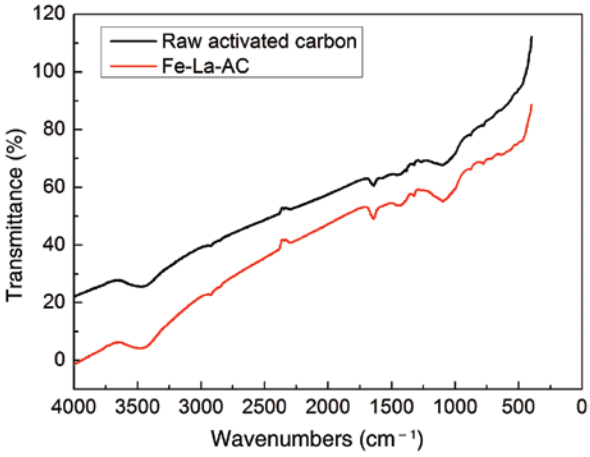

Figure 3: FTIR spectra of the raw activated carbon and Fe-La-AC.

function groups of raw activated carbon and Fe-La-AC can be obtained in Figure 3. As Figure 3 shows, there is a small difference in the general shape between raw activated carbon and Fe-La-AC. The spectra of raw activated carbon and Fe-La-AC have four obvious peaks at 3450, 1640, 1290, and 1110 cm^{-1}. The band at approximately 3450 cm^{-1} can be assigned to the O-H stretching vibration mode of hydroxyl functional groups, and the band at 1640 cm^{-1} can be assigned to the C=C symmetrical stretching of pyrone and the C=O of carboxylic groups [30, 31]. The peak at 1290 and 1110 cm^{-1} can be assigned to -C-O (eater, ether and phenol) and C-O functional [32].

3.3 Raman analysis

The Raman spectrum is applied to getting the information about the molecular vibration or rotational energy of the sample, reflecting the degree of structural disorder. In particular, the Raman spectrum is widely used to characterize the structure features of carbonaceous materials [33, 34]. The Raman spectra for raw activated carbon and

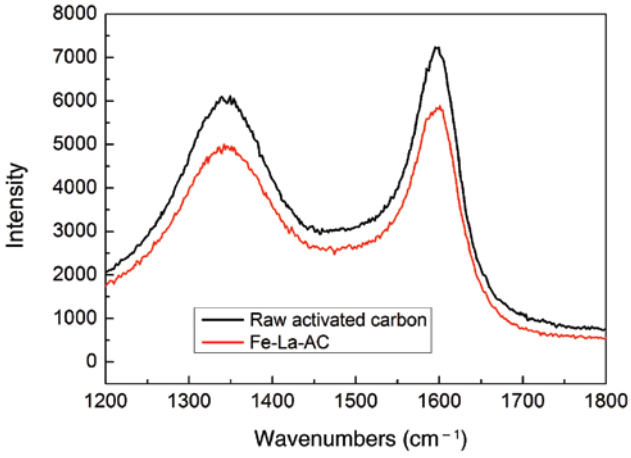

Figure 4: Raman spectrum for raw activated carbon and Fe-La-AC.

Fe-La-AC are shown in Figure 4. All the samples have two obvious D and G bands, which are assigned to the chaos and defection of crystalline structure and the graphitic structure of carbon materials, respectively [35, 36]. The two prominent peaks appear at approximately 1350 cm^{-1} (D band) and 1600 cm^{-1} (G band), which are the typical spectra of carbon materials (Figure 4). The value of R (I_D/I_G) is defined to characterize the disordering degree of carbon materials [37]. I_D and I_G are calculated for the integral intensities of the D and G peaks of the Raman spectrum, respectively [37]. The I_D/I_G value of the Fe-La-AC is larger than that of the raw activated carbon, indicating that the preparation process of Fe-La-AC slightly ruined the structure of graphite crystallite. This also means that the degree of graphitization of Fe-La-AC decreases because iron oxide and lanthanum oxide occupy the pore channel.

3.4 X-ray diffraction (XRD) spectra analyses

Figure 5 shows the XRD spectra of raw activated carbon and Fe-La-AC. As shown in Figure 5A, the main components of raw activated carbon are carbon, having three major peaks with numerous clutter peaks. Compared with Figure 5A, Fe-La-AC has relative smooth diffraction peak without many chaotic diffraction peaks. According to Figure 5B, Fe-La-AC has three substances (C, Fe_2O_3, and Fe_3O_4). It is determined that $Fe(NO_3)_3$ is successfully installed on the surface of activated carbon and subsequently decomposed iron oxides. However, there are no obvious peaks of lanthanum oxide because of the low lanthanum oxide contents. The Fe-La-AC is prepared by a $Fe(NO_3)_3/La(NO_3)_3$ mole ratio of 1 : 5, as shown in Figure 5C.

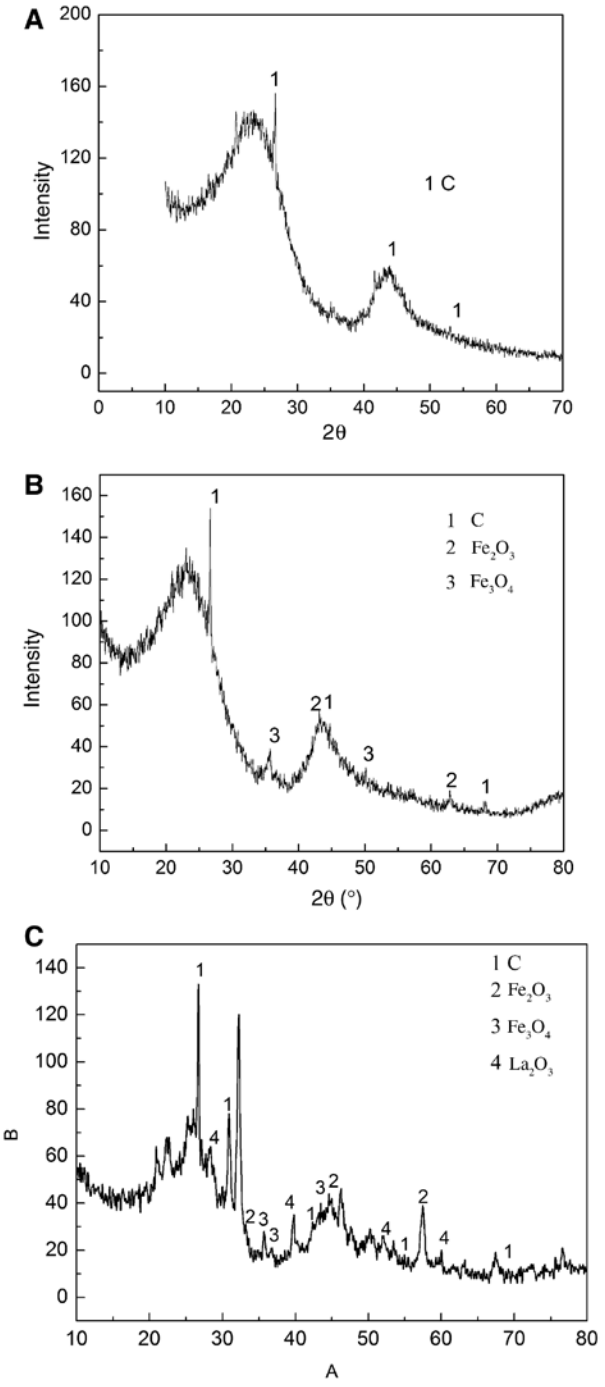

Figure 5: XRD spectra of the (A) raw activated carbon (B) Fe-La-AC ($Fe(NO_3)_3$/$La(NO_3)_3$ mole ratio of 1:5) and (C) Fe-La-AC ($Fe(NO_3)_3$/$La(NO_3)_3$ mole ratio of 4:2).

As shown in Figure 5C, we can observe that the La_2O_3 exists besides C, Fe_2O_3, and Fe_3O_4. Compared with Figure 5A–C, the peak intensity of Fe-La-AC is weak, indicating that the crystal structure of Fe-La-AC is not very obvious because of the part of the iron oxides and lanthanum oxide occupying the pores. The results are consistent with that of the Raman analysis.

3.5 XPS technique analyses

To further illuminate the composition and surface groups of Fe-La-AC, XPS technique is used. As shown in Figure 6A, the wide scan XPS technique of the Fe-La-AC indicates the existence of La, Fe, O, and C. Figure 6B shows the high resolution Fe 2p scan of Fe-La-AC. As shown in Figure 6B, the peaks at 711.2 and 725.5 eV associate with the binding energies of Fe 2p3/2 and Fe 2p1/2, respectively. The reported values for Fe^{2+} 2p3/2 and Fe^{3+} 2p3/2 are 709 and 711 eV, respectively [38]. Although, in this work, peak at a binding energy of approximately 711.2 eV in Fe-La-AC corresponds to the Fe 2p3/2 photoelectron peaks of iron oxides [39, 40], confirming that both ferrous and ferric oxides are present. Figure 6C presents the analysis of the La3d core level spectra, confirming that lanthanum exists. Details of the analysis procedure are given elsewhere [41]. Figure 6D shows the photoelectron peaks from O1s, which is resolved into four peaks. The peak approximately 530.7 eV is assigned to the oxygen in Fe-O of Fe-La-AC, indicating the existence of iron oxides. The deconvolution of O1s signal resulted in the understanding of the presence of lanthanum oxide at binding energies of 530.7 eV [42, 43]. The oxygen containing functional groups (hydroxyl groups) in graphene exists at approximately 531.8 eV [44]. The peak at the 532.2 eV arises from oxygen chemisorbed on the surface in other forms such as CO, CO_2, or grain boundary impurities [45, 46]. The result is in good agreement with XRD analysis.

3.6 Microscopic structure analysis

Figure 7A–C are the SEM images of raw activated carbon, ultrasound-activated carbon, and Fe-La-AC, respectively. It can be seen from Figure 7A that the pore structure of raw activated carbon is not clearly, and its surface is covered by a large amount of impurities. As shown in Figure 7B, the surface of ultrasound-activated carbon is clearly. Besides, the pore structure is also easily to see via ultrasound treatment. The pore structure of Fe-La-AC is clear (Figure 7C). However, the surface of Fe-La-AC should be covered with a layer of thin film, which may be Fe_2O_3, Fe_3O_4, and La_2O_3. The results are in good agreement with XRD.

3.7 Adsorption isotherms

Adsorption isotherms play a vital role in describing the adsorption mechanism and explain how adsorbate

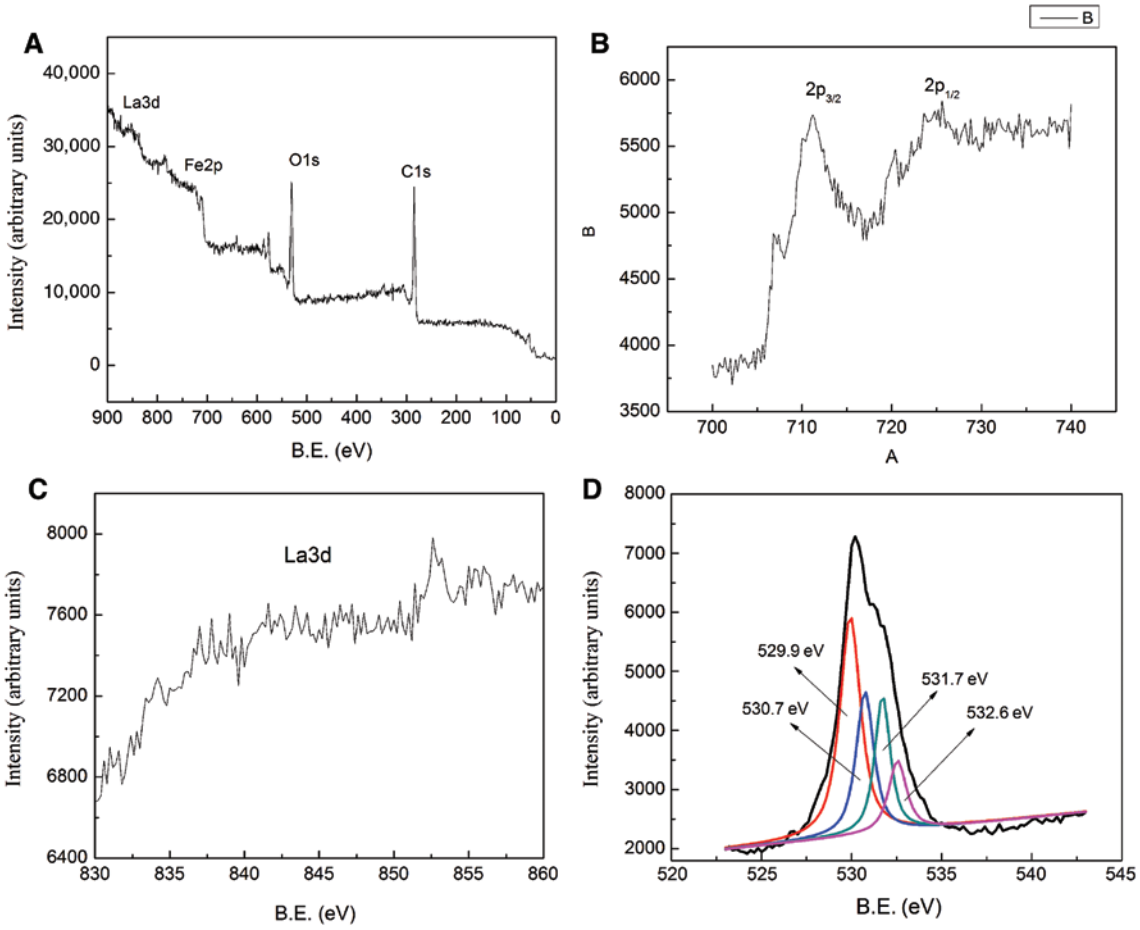

Figure 6: (A) The wide scan XPS spectrum, (B) the Fe 2p peaks, (C) the La 3d peaks, and (D) the O1s peaks of Fe-La-AC.

molecules in adsorbents are distributed under the adsorption equilibrium conditions. In this work, three isotherm models were used to determine which one is best match with the adsorption process. The adsorption parameters of these models for raw activated carbon and Fe-La-AC are calculated and summarized in Table 5. According to the results, the model correlation (R^2) value of the Langmuir isotherm is largest as compared with the Freundlich and Temkin isotherms. Moreover, another characteristic parameter of the Langmuir isotherm that can be used to evaluate the feasibility of adsorption on adsorbent is the dimensionless factor R_L called separation factor. It can be calculated by the following equation:

$$R_L = \frac{1}{1 + K_L C_0}, \tag{3}$$

where C_0 corresponds to the initial concentration of MB and K_L is the Langmuir constant. The value of R_L is related to the type of isotherm: unfavorable ($R_L > 1$), linear ($R_L = 1$), favorable ($0 < R_L < 1$), and irreversible ($R_L = 0$) [47]. The R_L values of the MB adsorption in adsorbents are calculated to be in the range of 0.0024–0.0105 for raw activated carbon and 0.0047–0.0153 for Fe-La-AC. Hence, the Langmuir isotherm is the best appropriate matching with the experiment data for both raw activated carbon and Fe-La-AC. These findings also suggest the homogeneous and the monolayer coverage of MB on the surface of raw activated carbon and Fe-La-AC. As shown in Table 5, the maximum monolayer adsorption capacity of Fe-La-AC is larger than that of raw activated carbon, indicating that the preparation method of Fe-La-AC is feasible. Fe-La-AC can be as effective adsorbent for MB removal. Besides, the adsorbed amount of MB increases as temperature increases, suggesting that the adsorption process is endothermic in nature. Theydan and Ahmed [48] also reported a similar trend. The reason is that the temperature increase also causes the increase in surface activity and kinetic energy, resulting in the interaction forces between the solute and the adsorbent to become stronger than the solute and the solvent [48]. Figure 8 shows the MB adsorption in the raw activated

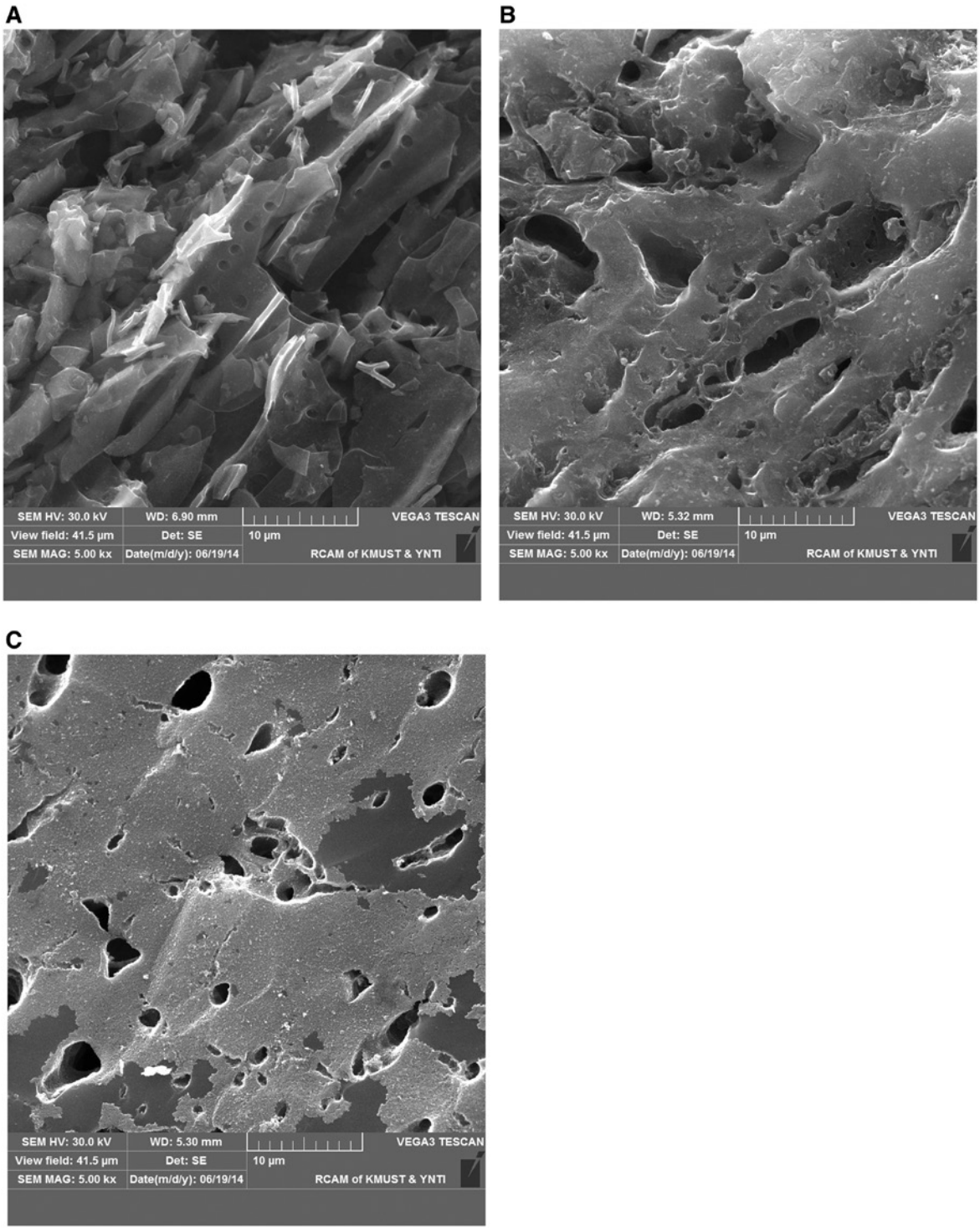

Figure 7: SEM images of the (A) raw activated carbon, (B) ultrasound-activated carbon, and (C) Fe-La-AC.

carbon and Fe-La-AC for the Langmuir isotherm at different temperatures.

Table 6 summarizes the maximum MB monolayer adsorption capacity of various adsorbents. In this work, the Q_0 of Fe-La-AC is larger than those reported [49–54]. The preparation process of Fe-La-AC is environment friendly, easy and energy saving and fast. So the Fe-La-AC can be easily large-scale production. Besides, Fe-La-AC having Fe_3O_4 leads to it having magnetic properties, which makes it easily separated and recycled from dye

Table 5: Adsorption isotherm parameters for the adsorption of raw-activated carbon and Fe-La-AC at different temperatures.

	Temperature (°C)	Langmuir			Freundlich			Temkin
		K_L (l/mg)	Q_0 (mg/g)	R^2	$1/n$	lnK_F	R^2	R^2
Raw activated carbon	30	0.477	178.25	0.999	0.194	4.718	0.879	0.954
	40	0.685	192.31	0.999	0.191	4.683	0.893	0.959
Fe-La-AC	30	0.322	254.45	0.995	0.196	4.755	0.874	0.952
	40	0.355	261.10	0.996	0.187	4.724	0.873	0.957

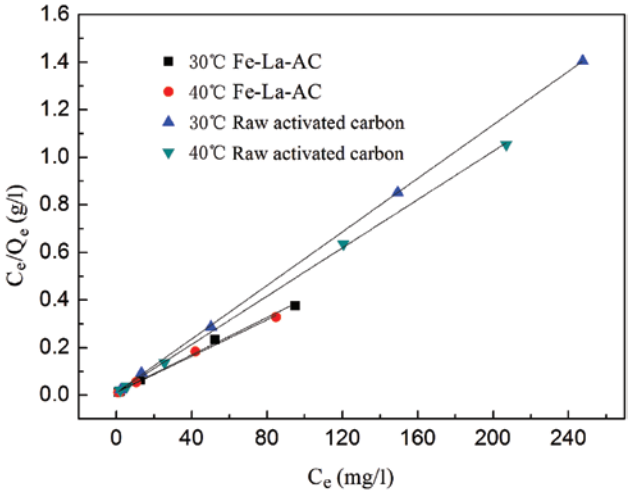

Figure 8: Langmuir isotherms for MB adsorption in raw activated carbon and Fe-La-AC at different temperatures.

Table 6: The maximum monolayer adsorption capacity of various adsorbents for MB.

Adsorbents	Maximum monolayer adsorption capacity (mg/g)	References
Fe-La-AC	261.10	This study
Raw activated carbon	192.31	This study
MCNCs-050	52.91	[49]
ZnS : Cu-NP-AC	123.46	[50]
Euphorbia rigida carbon	114.45	[51]
Fe_3O_4@GPTMS@Lys	185	[52]
Ag-NP-AC	71.43	[53]
CuO-NP-AC	10.55	[54]

MCNCs, magnetic colloidal nanocrystal clusters.

wastewater in an external magnetic field. In addition, the maximum adsorption capacity of Fe-La-AC is 261.10 mg/g, which increases by 26.38% as compared with raw activated carbon. Thus, Fe-La-AC can be as an effective adsorbent for the current dye industry based on the previously mentioned reasons.

3.8 Adsorption kinetics

The adsorption rate is a vital parameter and applied to describe the adsorption process. Many applications, including wastewater treatment, decoloring process, and organic pollution removal, all need a short adsorption time and rapid adsorption rate. Three models have been used to research the adsorption kinetics. Therefore, it is necessary to determine which models were most suitable for the adsorption data. The parameters of the three models for both raw activated carbon and Fe-La-AC are calculated and summarized in Table 7. The parameters of the three models can help us to predict the adsorption rate and to obtain many important information for designing and modeling the processes. As shown in Table 7, we find that the experimental data are consistent with the pseudo-second-order kinetic model with an R^2 value close to 1, for both raw activated carbon and Fe-La-AC. According to Table 7, we found that the adsorption rate K_2 of pseudo-second-order model decrease with the temperature increasing. The phenomenon shows that the adsorption process is more easily occurred at low temperature. On the whole, the K_2 for Fe-La-AC is larger than that of raw activated carbon. This proves that Fe-La-AC has larger adsorption rate, indicating that Fe-La-AC has good performance. Figure 9 shows the pseudo-second-order model for the adsorption of MB in raw activated carbon and Fe-La-AC at 400 ml/l under different temperatures.

The intraparticle diffusion model given by Weber and Morris is also usually used to further investigate the rate-limiting step of the adsorption process [55]. The MB is governed by either the intraparticle mass transport rate or the liquid phase mass transport rate [56, 57]. Compared with the pseudo-first order and pseudo-second order, intraparticle diffusion has the lower R^2 value. In other words, the intraparticle diffusion is unable to accurately predict MB adsorption in adsorbents. The results also prove that intraparticle diffusion is not the dominating factor in the MB adsorption process.

Table 7: Kinetic and intraparticle diffusion parameters for the adsorption of raw-activated carbon and Fe-Ce-AC at different temperatures.

Temperature (°C)	Pseudo-first order			Pseudo-second order		
	K_1 (min^{-1})	R^2	Q_e	K_1 (min^{-1})	R^2	Q_e
30	0.00133	0.977	112.285	0.00276	0.994	65.581
40	0.00221	0.956	71.516	0.01777	0.980	45.997
	K_1 (min^{-1})	R^2	Q_e (mg/g)	Q_e (mg/g)	R^2	K_2 (g/mg^1/min^1)
30	0.0029	0.994	62.665	203.666	0.999	0.0012
40	0.0195	0.940	39.629	172.710	0.997	0.0006
	Intraparticle diffusion			Intraparticle diffusion		
	C (mg/g)	K_3 (mg/g/min$^{1/2}$)	R^2	C (mg/g)	K_3 (mg/g/min$^{1/2}$)	R^2
30	169.848	2.354	0.836	165.17	2.679	0.917
40	128.281	2.769	0.954	128.237	2.547	0.978

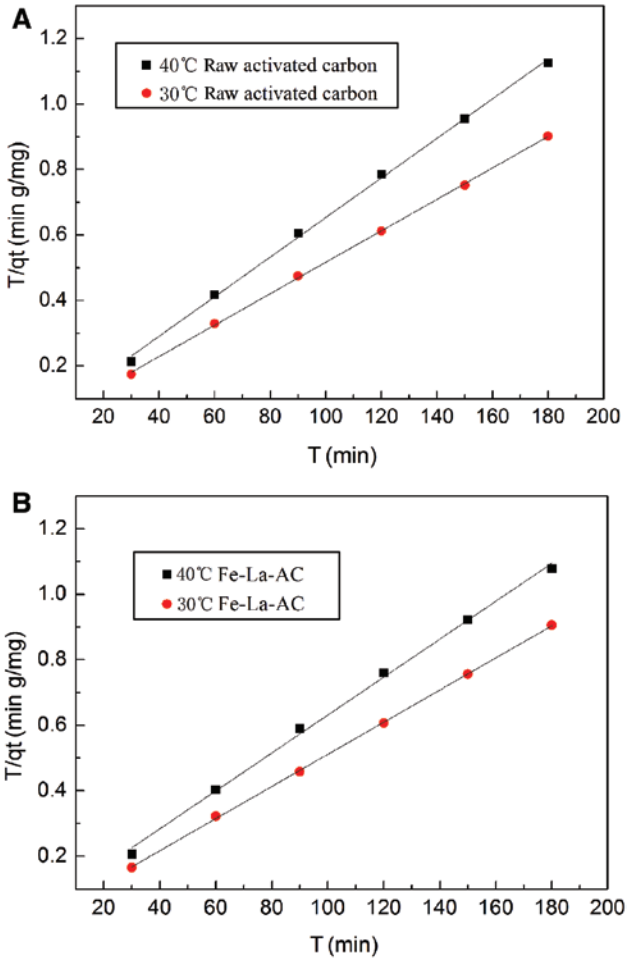

Figure 9: Pseudo-second-order kinetics for the adsorption of MB in (A) raw activated carbon and (B) Fe-La-AC at different temperatures.

4 Conclusion

The Fe-La-AC was prepared by microwave heating under ultrasonic pretreatment condition and exhibited well MB removal capacity. In this work, the physicochemical properties of Fe-La-AC have been characterized by N_2 adsorption, FTIR, Raman, XRD, XPS, and SEM. The surface chemistry and the textural properties of Fe-La-AC changed when it was modified by iron nitrate and lanthanum nitrate by microwave heating. Moreover, the existence of Fe_3O_4 leads to Fe-La-AC having magnetic properties, which makes it easily separated and recycled from dye wastewater in an external magnetic field. The MB removal efficiency is significantly improved as compared with raw activated carbon with maximum adsorption capacity of 261.10 mg/g. In addition, adsorption isotherms and adsorption kinetics were thorough studied for the dye wastewater treatment. The equilibrium data fit well with the Langmuir model, and the kinetic data tend to match well in the pseudo-second-order model. The above-mentioned analyses proved the successful application of Fe-La-AC for effective removal of MB, providing a new promising adsorbent for dye wastewater.

Acknowledgments: The authors express their gratitude to the Specialized Research Fund of the National Natural Science Foundation of China (grant nos. 51504119 and 21567013), National High Technology Research and Development Plan (grant no. 2015AA020201, 863 Program) the Yunnan Applied Basic Research Project (grant no. 2015FB129), and the Yunnan Provincial Science and Technology Innovation Talents Scheme Technological Leading Talent (grant no. 2013HA002).

References

[1] Nethaji S, Sivasamy A. *Chemosphere* 2011, 82, 1367–1372.
[2] Ghaedi M, Nasab AG, Khodadoust S, Sahraei R, Daneshfar A. *J. Ind. Eng. Chem.* 2015, 21, 986–993.

[3] Rosenkranz HS, Cunningham SL, Mermelstein R, Cunningham AR. *Mutat. Res. Genet. Toxicol. Environ. Mutagen*. 2007, 633, 55–66.
[4] Mirzaei A, Ebadi A, Khajavi P. *Chem. Eng. J.* 2013, 231, 550–560.
[5] Ghaedi M, Ghayedi M, Kokhdan SN, Sahraei R, Daneshfar A. *J. Ind. Eng. Chem.* 2013, 19, 1209–1217.
[6] Yao YJ, Xu FF, Chen M, Xu ZX, Zhu ZW. *Bioresour. Technol.* 2010, 101, 3040–3046.
[7] Kayan B, Gözmen B, Demirel M, Gizir AM. *J. Hazard. Mater.* 2010, 177, 95–102.
[8] Tünay O, Kabdasli I, Eremektar G, Orhon D. *Water Sci. Technol.* 1996, 34, 9–16.
[9] Forgacsa E, Cserhátia T, Oros G. *Environ. Int.* 2004, 30, 953–971.
[10] Qianqian Z, Tang B, Guoxin H. *J. Hazard. Mater.* 2011, 198, 78–86.
[11] Tehrani-Bagha AR, Mahmoodi NM, Menger FM. *Desalination* 2010, 260, 34–38.
[12] Alventosa-deLara E, Barredo-Damas S, Alcaina-Miranda MI, Iborra-Clar MI. *J. Hazard. Mater.* 2012, 209–210, 492–500.
[13] Robinson T, McMullan G, Marchant R, Nigam P. *Bioresour. Technol.* 2001, 77, 247–255.
[14] Ghaedi M, Hajati S, Barazesh B, Karimi F, Ghezelbash G. *J. Ind. Eng. Chem.* 2013, 19, 227–233.
[15] Asfaram A, Ghaedi M, Hajati S, Goudarzi A, Bazrafshan AA. *Spectrochim. Acta A Mol. Biomol. Spectrosc.* 2015, 145, 203–212.
[16] Liu SL, Wang YN, Lu KT. *J. Porous Mater.* 2014, 21, 459–466.
[17] Policicchio A, Maccallini E, Agostino RG. *Fuel* 2013, 104, 813–821.
[18] Ge XY, Zhansheng W, Zhilin W, Yujun Y, Giancarlo G, Bang-Ce Y. *J. Taiwan Inst. Chem. Eng.* 2016, 64, 235–243.
[19] Dong Y, Lin HM, Qu FY. *Chem. Eng. J.* 2012, 193–194, 169–177.
[20] Goscianska J, Marciniak M, Pietrzak R. *Chem. Eng. J.* 2014, 247, 258–264.
[21] Shah I, Adnan R, Saime W, Ngah W, Mohamed N, Taufiq-Yap YH. *Bioresour. Technol.* 2014, 160, 52–56.
[22] Wang ZH, Shen DK, Shen F, Li TY. *Chemosphere* 2016, 150, 1–7.
[23] Zhang L, Wan LH, Chang N, Liu JY, Duan C, Zhou Q, Li XL, Wang XZ. *J. Hazard. Mater.* 2011, 190, 848–855.
[24] Kadirova ZC, Katsumata K, Isobe T, Matsushita N, Nakajima A, Okada K. *J. Environ. Chem. Eng.* 2014, 2, 2026–2036.
[25] Su Y, Yang WY, Sun WZ, Li Q, Shang JK. *Chem. Eng. J.* 2015, 268, 270–279.
[26] Ren ZM, Shao LN, Zhang GS. *Water Air Soil Pollut.* 2012, 223, 4221–4231.
[27] Cheng S, Zhang LB, Xia HY, Zhang SZ, Peng JH, Wang SX. *J. Porous. Mater*. 2016, 23, 1–11.
[28] Cheng S, Zhang LB, Xia HY, Zhang SZ, Peng JH, Shu JH, Li CY. *RSC Adv.* 2016, 6, 78936–78946.
[29] Kasaoka S, Sakata Y, Tanaka E, Naitoh R. *Int. Chem. Eng.* 1989, 29, 734–742.
[30] Ji YB, Li TH, Zhu L. *Appl. Surf. Sci*. 2007, 254, 506–512.
[31] Moniruzzaman M, Ono T. *Bioresour. Technol.* 2013, 127, 132–137.
[32] Foo KF, Hameed BH. *Chem. Eng. J.* 2012, 180, 66–74.
[33] Sadezky A, Muckenhuber H, Grothe H, Niessner R, Pöschl U. *Carbon* 2005, 43, 1731–1742.
[34] Xu X, Song W, Huang DG, Gao BY, Sun YY, Yue QY, Fu KF. *Colloids Surf. A Physicochem. Eng. Asp.* 2015, 476, 68–75.
[35] Nemanich RJ, Solin SA. *Phys. Rev. B*. 1979, 20, 392–401.
[36] Zhou XX, Qu X, Zhang R, Bi JC. *Fuel Process. Technol.* 2015, 135, 195–202.
[37] Yao SH, Zhang JJ, Shen DK, Xiao R, Gu S, Zhao M, Liang JY. *J. Colloid Interface Sci.* 2016, 463, 118–127.
[38] Tong M, Yuan S, Long H, Zheng M, Wang L, Chen J. *J. Contam. Hydrol*. 2011, 122, 16–25.
[39] Xi YF, Sun ZM, Hreid T, Ayoko GA, Frost RL. *Chem. Eng. J.* 2014, 247, 66–74.
[40] Chen H, Luo H, Lan Y, Dong T, Hu B, Wang YJ. *Hazard Mater*. 2011, 192, 44–53.
[41] Tonti D, Martinez L, Torralvo MJ, Enciso E, Roman E, Sanz J. *J. Electrochem. Soc.* 2010, 157, B1499–B1504.
[42] Zou P, Yao MW, Chen JW, Peng Y, Yao X. *Ceram. Int.* 2016, 42, 4120–4125.
[43] Shi L, Yuan Y, Liang XF, Xia YD, Yin J, Liu ZG. *Appl. Surf. Sci.* 2007, 253, 3731–3735.
[44] Li Y, Zhang RF, Tian XK, Yang C, Zhou ZX. *Appl. Surf. Sci*. 2016, 369, 11–18.
[45] Murugan R, Vijayaprasath G, Ravi G. *Superlattices Microstruct.* 2015, 85, 321–330.
[46] Kotani A, Haruhiko O. *J. Electron Spectrosc. Relat. Phenom.* 1992, 60, 257.
[47] Guo S, Li W, Zhang L, Peng J, Xia H, Zhang S. *Process Saf. Environ. Prot.* 2009, 87, 343–351.
[48] Theydan KS, Ahmed MJ. *J. Anal. Appl. Pyrolysis* 2012, 97, 116–122.
[49] Song YB, Lv SN, Cheng CJ, Ni GL, Xie XW, Huang W, Zhao ZG. *Appl. Surf. Sci*. 2015, 324, 854–863.
[50] Gao P, Liu ZH, Xue G, Han B, Zhou MH. *Bioresour. Technol.* 2011, 102, 3645–3648.
[51] Cercel O, Ozcan A, Ozcan AS, Gercel HF. *Appl. Surf. Sci*. 2007, 253, 4843–4852.
[52] Haque E, Jun JW, Jhung SH. *J. Hazard. Mater.* 2011, 185, 507–511.
[53] Zhang YR, Shen SL, Wang SQ, Huang J, Su P, Wang QR, Zhao BX. *Chem. Eng. J.* 2014, 239, 250–256.
[54] Mahapatra K, Ramteke DS, Paliwal LJ. *J. Anal. Appl. Pyrolysis* 2012, 95, 79–86.
[55] Jagtap S, Yenkie MK, Das S, Rayalu S. *Desalination* 2011, 273, 267–275.
[56] Ghaedi M, Ghaedi AM, Hossainpour M, Ansari A, Habibi MH, Asghari AR. *J. Ind. Eng. Chem.* 2014, 20, 1641–1649.
[57] Foo KF, Hameed BH. *Chem. Eng. J.* 2011, 173, 385–390.

Bionotes

Song Cheng

Song Cheng is a PhD candidate at Kunming University of Science and Technology. He mainly engages in microwave heating in the application of chemical engineering and materials.

Libo Zhang

Libo Zhang is a PhD supervisor at Kunming University of Science and Technology. He mainly engages in microwave heating in the application of metallurgy, chemical engineering, and materials.

Hongying Xia

Hongying Xia is an Associate Professor at Kunming University of Science and Technology. He mainly engages in microwave heating in the application of metallurgy, chemical engineering, and materials.

Jinhui Peng

Jinhui Peng is a PhD supervisor at Kunming University of Science and Technology. He mainly engages in microwave heating in the application of metallurgy, chemical engineering, and materials science. He has received many awards, among which are the State Technological Invention Award and the Natural Science Award of Kunming province.